

OTFS Signaling for SCMA With Coordinated Multi-Point Vehicle Communications

Yao Ge, *Member, IEEE*, Qinwen Deng, *Student Member, IEEE*, David González G., *Senior Member, IEEE*, Yong Liang Guan, *Senior Member, IEEE*, and Zhi Ding, *Fellow, IEEE*

Abstract—This paper investigates an uplink coordinated multi-point (CoMP) coverage scenario, in which multiple mobile users are grouped for sparse code multiple access (SCMA), and served by the remote radio head (RRH) in front of them and the RRH behind them simultaneously. We apply orthogonal time frequency space (OTFS) modulation for each user to exploit the degrees of freedom arising from both the delay and Doppler domains. As the signals received by the RRHs in front of and behind the users experience respectively positive and negative Doppler frequency shifts, our proposed OTFS-based SCMA (OBSCMA) with CoMP system can effectively harvest extra Doppler and spatial diversity for better performance. Based on maximum likelihood (ML) detector, we analyze the single-user average bit error rate (ABER) bound as the benchmark of the ABER performance for our proposed OBSCMA with CoMP system. We also develop a customized Gaussian approximation with expectation propagation (GAEP) algorithm for multi-user detection and propose efficient algorithm structures for centralized and decentralized detectors. Our proposed OBSCMA with CoMP system leads to stronger performance than the existing solutions. The proposed centralized and decentralized detectors exhibit effective reception and robustness under channel state information uncertainty.

Index Terms—Centralized and decentralized detector, CoMP, SCMA, OTFS, Performance analysis, V2X.

I. INTRODUCTION

The demand for the variety and the number of mobile devices along with the mobile communication applications have increased tremendously. Communications in high-mobility scenarios such as high-speed railways and vehicle-to-everything (V2X) suffer from the well-known time-varying channels with high Doppler spread [1]. Traditional orthogonal frequency division multiplexing (OFDM) systems experience significant performance loss due to the severe inter-carrier-interference (ICI) caused by the channel Doppler spread. The recent emergence of orthogonal time frequency space (OTFS) modulation [2] can exploit the degrees of freedom coming from both the delay and Doppler channel domains, resulting

This study is supported under the RIE2020 Industry Alignment Fund—Industry Collaboration Projects (IAF-ICP) Funding Initiative, as well as cash and in-kind contribution from the industry partner(s). The work of Qinwen Deng and Zhi Ding was supported in part by the National Science Foundation under Grant 2029027.

Yao Ge and Yong Liang Guan are with the Continental-NTU Corporate Lab, Nanyang Technological University, Singapore (e-mail: yao.ge@ntu.edu.sg; eylguan@ntu.edu.sg). Yong Liang Guan is also with the School of Electrical and Electronics Engineering, Nanyang Technological University, Singapore.

Qinwen Deng and Zhi Ding are with the Department of Electrical and Computer Engineering, University of California at Davis, Davis, CA 95616 USA (e-mail: mrdeng@ucdavis.edu; zding@ucdavis.edu).

David González G. is with the Wireless Communications Technologies Group, Continental AG, Germany (e-mail: david.gonzalez.g@ieee.org).

in superior performance and more reliable communications compared to OFDM. OTFS can effectively simplify channel estimation [3]–[5] and symbol detection [6]–[9] at wireless receivers by utilizing the property of a quasi-stationary sparse channel in delay-Doppler domain for high-mobility communication scenarios. The performance of uncoded and coded OTFS systems has been analyzed and evaluated in [10]–[12] and [13], respectively.

Meanwhile, efficient multiple access protocols represent another strong arena of growth. Recently, several works [14]–[16] investigated multiple mobile user access based on OTFS framework with orthogonal resource allocation. In [14], [15], the authors proposed to allocate different time-frequency resources to different mobile users with certain impractical assumptions specially the availability of the elusive ideal bi-orthogonal pulses. The authors in [16] allocated different delay-Doppler resources to different mobile users and developed efficient receiver algorithm to tackle the significant co-channel interference (CCI).

To further support massive multiple access and explosive transmission needs, non-orthogonal multiple access (NOMA) has been considered as a promising solution for high spectrum efficiency in traditional overloaded multi-user OFDM [17] and multiple-input multiple-output (MIMO) [18] systems. Existing NOMA methods are mainly categorized into power-domain and code-domain NOMA [19], [20]. In particular, sparse code multiple access (SCMA) [21]–[24] is a code-domain NOMA, which has attracted tremendous research attention due to its excellent performance and low receiver complexity. The application of NOMA to OTFS can effectively improve spectrum utilization and support massive mobile connectivity [25]–[28]. In OTFS-NOMA, multiple mobile users are allowed to share the same delay-Doppler resources simultaneously, and distinguished by either different power levels [25] or with the help of sparse codewords [26]. The authors in [27] proposed to pair an OTFS mobile user with a group of OFDM stationary users for the implementation of NOMA. Unlike [27], a recent work [28] suggested an OTFS-based NOMA (OBNOMA) configuration, where multiple stationary users and multiple mobile users are grouped for non-orthogonal channel sharing via only using OTFS modulation. The proposed OBNOMA framework and developed advanced receiver algorithms in [28] can effectively address the CCI and recover the signal for each user.

In addition, multiple antenna systems [29], [30] have gained overwhelming research interest in the last several decades both in academia and industry. The integration of OTFS

with MIMO systems can acquire additional diversity, multiplexing, and antenna gains compared to conventional single antenna systems [31]–[38]. In [31], the authors proposed a low-complexity detector and low-overhead pilot pattern for OTFS system with a large-scale antenna array at the receiver. A Bayesian learning aided simultaneous row and group sparse channel estimation method was proposed in [32] and an efficient symbol detection scheme was proposed in [33] for MIMO-OTFS systems. The authors in [34] applied a deterministic pilot pattern and developed an efficient channel estimation scheme for downlink massive MIMO-OTFS systems. An uplink-aided high mobility downlink channel estimation method was proposed in [35] for massive MIMO-OTFS networks. The work in [36] analyzed and evaluated the performance of linear receivers for MIMO-OTFS systems. The authors in [37] proposed a low complexity multi-user precoding and detector for downlink massive MIMO-OTFS systems. A novel path division multiple access (PDMA) was proposed in [38], where the additional angle-domain can be utilized to differentiate mobile users for massive MIMO-OTFS networks.

However, most of the existing works do not fully utilize the potential performance gain by applying restriction to co-located MIMO designs. To preserve sufficient diversity and exploit favorable propagation property of mobile communications, we shall apply distributed antenna systems with coordinated multi-point (CoMP) transmission and reception. CoMP system was originally proposed to improve average spectral efficiency and alleviate interference between inter-cells in traditional cellular networks [39]. Here, we adopt CoMP operation between the neighbouring remote radio heads (RRHs) for better exploit of the diversity. Without loss of generality, we focus on a specific scenario in which multiple mobile users are grouped for SCMA, and served by the RRH in front of them and the RRH behind them simultaneously. As the signals received by the RRHs in front of and behind the users experience respectively positive and negative Doppler frequency shifts, we propose an OTFS-based SCMA (OBSCMA) with CoMP system to acquire additional diversity coming from Doppler and spatial domain. Due to the sufficient diversity, our proposed OBSCMA with CoMP system can achieve significant performance improvement over its OFDM-based SCMA (OFDM-SCMA) counterparts [40] for high-mobility communications.

Specifically, we propose an OBSCMA with CoMP system to support multiple mobile users connectivity, and exploit the underlying channel diversity for better performance. We also develop efficient practical receivers to mitigate CCI and recover the signal for each user. The contributions of our work are summarized as follows:

- 1) We propose an OBSCMA with CoMP configuration, where a group of SCMA mobile users modulated in accordance with OTFS, and served by the RRH in front of them and the RRH behind them simultaneously. The proposed system framework can naturally harvest sufficient diversity coming from both the delay, Doppler and spatial domain, and is amenable to effective receiver algorithms.

- 2) Based on the maximum likelihood (ML) detector, we analyze the single-user pairwise error probability (PEP) and characterize its average bit error rate (ABER) bound as the benchmark of the ABER performance for our OBSCMA with CoMP system. From the ABER analysis, the performance improvement of the proposed scheme is evaluated.
- 3) We develop a practical customized Gaussian approximation with expectation propagation (GAEP) algorithm for multi-user detection. We also propose efficient algorithm structures for centralized and decentralized GAEP detectors to take advantage of underlying channel diversity from the receptions of the RRHs.
- 4) We demonstrate that our proposed OBSCMA with CoMP system can achieve better performance than the existing solutions such as co-located RRHs and traditional cellular networks, as well as their OFDM-SCMA counterparts. The proposed decentralized detector converges to the results obtained by the centralized one, and both of them exhibit robustness to the imperfect channel state informations (CSIs).

The remainder of this paper is organized as follows. Section II introduces the system model of the proposed OBSCMA with CoMP system. Section III analyzes the single-user PEP and captures its ABER bound as the benchmark of the OBSCMA with CoMP system. In Section IV, we develop practical receiver algorithms for centralized and decentralized GAEP detectors, and also discuss about their advantages and disadvantages, respectively. The simulation results and discussions are presented in Section V. Finally, Section VI concludes our work.

Notations: Throughout this paper, we use boldface upper case letters to denote matrices and boldface lower case letters to denote vectors. The superscripts $(\cdot)^T$, $(\cdot)^H$ and $(\cdot)^{-1}$ stand for the transpose, conjugate transpose and inverse, respectively. $|\cdot|$ denotes the absolute value of a complex scalar or the cardinality of a set. $\Pr(\cdot)$ defines probability of an event and $Q(\cdot)$ is the tail distribution function of the standard Gaussian distribution. $\exp(\cdot)$ and $\mathbb{E}(\cdot)$ refer to natural exponential function and statistical expectation operation, respectively. $[\cdot]_N$ denotes the modulo N operation and $\lceil \cdot \rceil$ represents the round up operation. The imaginary unit is denoted by $j = \sqrt{-1}$. A complex Gaussian distribution with mean $\boldsymbol{\mu}$ and covariance $\boldsymbol{\eta}$ is denoted by $\mathcal{CN}(\boldsymbol{\mu}, \boldsymbol{\eta})$. $\mathbb{C}^{M \times N}$, \mathbf{I}_M and $\mathbf{0}_{M \times N}$ denote the $M \times N$ matrix with complex entries, $M \times M$ identity matrix and $M \times N$ zero matrix, respectively. $A[i, j]$ is the (i, j) -th entry of matrix \mathbf{A} and $a[i]$ is the i -th element of vector \mathbf{a} . $\text{diag}\{\mathbf{a}\}$ denotes a diagonal matrix whose main diagonal is \mathbf{a} . The matrix $\mathbf{F}_N = \left(\frac{1}{\sqrt{N}} e^{-j2\pi \frac{k\ell}{N}} \right)_{k, \ell=0, 1, \dots, N-1}$ represents the normalized N -point discrete Fourier transform (DFT) matrix. The big-O notation $\mathcal{O}(\cdot)$ asymptotically describes the order of computational complexity.

II. SYSTEM MODEL

In this section, we introduce the system model and mathematical expression of the proposed OBSCMA with CoMP

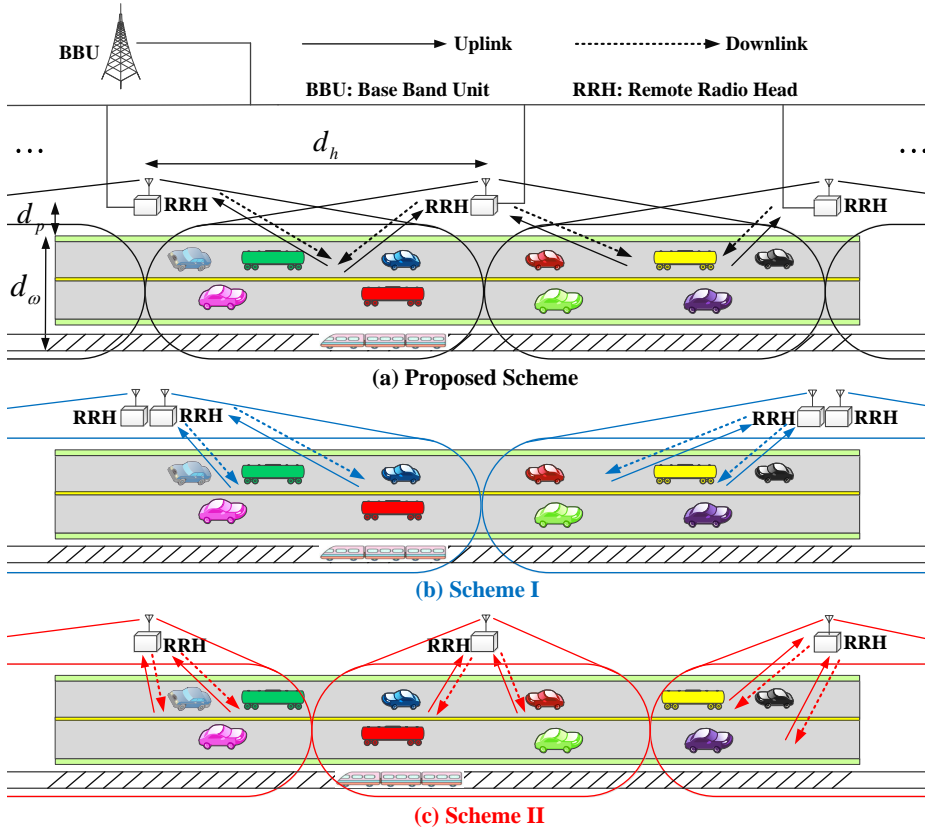


Fig. 1. Uplink system model. (a) Proposed OBSCMA with CoMP system. (b) Co-located RRHs Scheme (Scheme I). (c) Traditional cellular network scheme (Scheme II).

system, which includes the system description, transmitter model, channel model and receiver model, respectively.

A. System Description

We consider an uplink CoMP system shown in Fig. 1(a), where the base band unit (BBU) is connected with a serial of RRHs¹ by optical fibers. At each transmit slot, J independent mobile users located in the same cell, are served by the RRH in front of them and the RRH behind them simultaneously. To highlight the superiority of the proposed scheme, we also introduce the co-located RRHs scheme shown in Fig. 1(b) and traditional cellular network scheme shown in Fig. 1(c) as benchmarks. In particular, the RRHs are co-located deployed and the users are served by the nearest RRHs in Fig. 1(b), and the RRHs are distributed deployed and each one only serves the users in its own cell in Fig. 1(c). More detailed discussions and comparisons of the different schemes can be found in Section III and Section V.

The message from each user is mapped into a K -dimensional SCMA codeword. We assume that each user employs only one SCMA layer and $J > K$ typically, resulting in an overloading factor $\delta = \frac{J}{K} > 1$. We further assign the SCMA codewords over the delay-Doppler plane and adopt OTFS modulation for uplink transmission. Without loss of

generality, a lattice in delay-Doppler plane is denoted as

$$\Gamma = \left\{ \left(\frac{\ell}{M\Delta f}, \frac{k}{NT} \right), \ell = 0, \dots, M-1; k = 0, \dots, N-1 \right\},$$

and the corresponding time-frequency plane is given by

$$\Lambda = \{(m\Delta f, nT), m = 0, \dots, M-1; n = 0, \dots, N-1\},$$

where M and N denote, respectively, the total available numbers of subcarriers and time intervals. The choices of T and $\Delta f = 1/T$ (Hz) should be larger than the maximal channel delay spread and maximum Doppler frequency shift, respectively. To avoid unnecessary confusion, we use a simple model in which the mobile users and the RRH receivers are equipped with a single transmit antenna and receive antenna. It is worth mentioning that our proposed scheme also applies to the scenarios involving multiple transmit and receive antennas, with expected performance gain. We also emphasize that the performance advantages of the proposed scheme and algorithm still work for downlink scenario in a straightforward manner.

B. Transmitter Model

At the transmitter, every $\log_2 Q$ information bits \mathbf{b}_j from the j -th user are mapped into a complex K -dimensional sparse codeword $\mathbf{c}_j = [c_{j,1}, c_{j,2}, \dots, c_{j,K}]^T$ selected from a user-specific SCMA codebook \mathbb{A}_j of size Q , where $j = \{1, 2, \dots, J\}$. We assume that only $D < K$ non-zero entries among a K -dimensional codeword \mathbf{c}_j . We then generate the information symbols $\mathbf{X}_j \in \mathbb{C}^{M \times N}$ of the j -th user by

¹The terminology Road Side Unit (RSU) is also commonly found in vehicle communications.

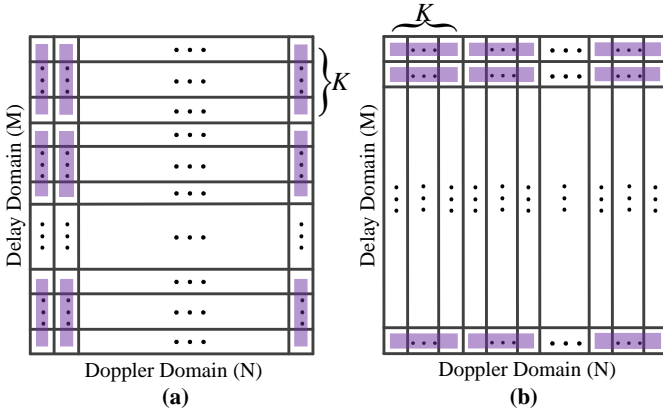


Fig. 2. SCMA codewords allocation. (a) Allocated along the delay axis. (b) Allocated along the Doppler axis.

allocating $\frac{MN}{K}$ SCMA codewords \mathbf{c}_j over the delay-Doppler plane Γ without overlapping.

In general, the SCMA codewords can be allocated either along the delay axis in Fig. 2(a) or along the Doppler axis in Fig. 2(b). For simplicity, here, we assume that M and N are integer multiples of K , i.e., $[M]_K = [N]_K = 0$, where $[\cdot]_k$ denotes mod- k operation.

The delay-Doppler symbols $\mathbf{X}_j \in \mathbb{C}^{M \times N}$ are then converted into a lattice in time-frequency domain $\tilde{\mathbf{X}}_j \in \mathbb{C}^{MN \times N}$ through the inverse symplectic finite Fourier transform (ISFFT) for each user,

$$\tilde{\mathbf{X}}_j = \mathbf{F}_M \mathbf{X}_j \mathbf{F}_N^H, \quad (1)$$

where $\mathbf{F}_M \in \mathbb{C}^{M \times M}$ and $\mathbf{F}_N \in \mathbb{C}^{N \times N}$ denote, respectively, the normalized M -point and N -point DFT matrices.

Next, each time-frequency signal $\tilde{\mathbf{X}}_j$ is transformed into a time domain signal $\mathbf{s}_j \in \mathbb{C}^{MN \times 1}$ through Heisenberg transform with a transmit pulse $g_{tx}(t)$,

$$\begin{aligned} s_j[c] &= \sum_{n=0}^{N-1} \sum_{m=0}^{M-1} \tilde{X}_j[m, n] g_{tx}(cT_s - nT) e^{j2\pi m \Delta f (cT_s - nT)}, \\ c &= 0, \dots, MN - 1, \end{aligned} \quad (2)$$

where $T_s = 1/M\Delta f$ is the sampling interval.

We then apply a cyclic prefix (CP) in front of the generated time domain signal for each user. After passing through a transmit filter, each mobile user signal is sent out over a doubly-selective fading channel.

C. Channel Model

In this work, we characterize the channel between j -th user and u -th RRH as

$$\begin{aligned} g_{uj}[c, p] &= \sqrt{PL(d_{uj})} h_{uj}[c, p], \quad c = 0, \dots, MN - 1; \\ p &= 0, \dots, P_{uj} - 1, \end{aligned} \quad (3)$$

where $PL(d_{uj})$ represents the distance-dependent pathloss, d_{uj} is the distance from j -th user to the u -th RRH,² and $u = \{1, 2\}$.

²We assume that the distance remains constant during an OTFS transmission frame.

In (3), \mathbf{h}_{uj} represents the time-varying multipath fading channel with sampled impulse response

$$h_{uj}[c, p] = \sum_{i=1}^{L_{uj}} h_{uj,i} e^{j2\pi \nu_{uj,i} (cT_s - pT_s)} \text{Pr}_c(pT_s - t_{uj} - \tau_{uj,i}), \quad (4)$$

where L_{uj} and t_{uj} denote the number of multipaths and the amount of timing offset between the j -th user and u -th RRH; $h_{uj,i}$, $\tau_{uj,i}$ and $\nu_{uj,i}$ are the corresponding channel gain, delay and Doppler frequency shift associated with the i -th path, respectively. The Doppler frequency shift of the i -th path can be further written as $\nu_{uj,i} = (k_{uj,i} + \beta_{uj,i})/NT$, where integer $k_{uj,i}$ and real $\beta_{uj,i} \in (-0.5, 0.5]$ denote the index and fractional part of $\nu_{uj,i}$, respectively.

The maximal channel tap P_{uj} is determined by the duration of the filter response and the maximum channel delay spread. In general, the implemented pulse shaping filters at the transmitter and receiver are the root-raised-cosine (RRC) filters, leading to an equivalent overall raised-cosine (RC) rolloff pulse for $\text{Pr}_c(\tau)$ in (4). In addition, we assume that the CP is long enough to accommodate both the maximum timing offset and the maximal channel delay spread for all users. Hence, there is no inter-frame interference.

D. Receiver Model

At the receiver, the CP is removed after the time domain signal enters a received filter. We can express the received signal from the j -th user at the u -th RRH as

$$r_{uj}[c] = \sum_{p=0}^{P_{uj}-1} g_{uj}[c, p] s_j [[c - p]_{MN}], \quad c = 0, \dots, MN - 1. \quad (5)$$

The resulting time domain signal $\mathbf{r}_{uj} \in \mathbb{C}^{MN \times 1}$ is then transformed into the time-frequency domain by Wigner transform with a receive pulse $g_{rx}(t)$,

$$\begin{aligned} \bar{Y}_{uj}[m, n] &= \sum_{c=0}^{MN-1} g_{rx}^*(cT_s - nT) r_{uj}[c] e^{-j2\pi m \Delta f (cT_s - nT)}, \\ m &= 0, \dots, M - 1; \quad n = 0, \dots, N - 1. \end{aligned} \quad (6)$$

Finally, the time-frequency signal $\bar{\mathbf{Y}}_{uj} \in \mathbb{C}^{M \times N}$ is transformed back to delay-Doppler domain via the symplectic finite Fourier transform (SFFT),

$$\mathbf{Y}_{uj} = \mathbf{F}_M^H \bar{\mathbf{Y}}_{uj} \mathbf{F}_N. \quad (7)$$

For analytical convenience, we adopt a rectangular pulse for $g_{tx}(t)$ and $g_{rx}(t)$ in the above steps, and express the baseband OTFS input-output relationship from j -th user to u -th RRH in delay-Doppler domain as [41]

$$\begin{aligned} Y_{uj}[\ell, k] &= \sqrt{PL(d_{uj})} \sum_{p=0}^{P_{uj}-1} \sum_{i=1}^{L_{uj}} \sum_{q=0}^{N-1} h_{uj,i} \text{Pr}_c(pT_s - t_{uj} - \tau_{uj,i}) \\ &\quad \times \gamma(k, \ell, p, q, k_{uj,i}, \beta_{uj,i}) X_j [[\ell - p]_M, [k - k_{uj,i} + q]_N], \end{aligned} \quad (8)$$

where

$$\begin{aligned} & \gamma(k, \ell, p, q, k_{uj,i}, \beta_{uj,i}) \\ &= \begin{cases} \frac{1}{N} \xi(\ell, p, k_{uj,i}, \beta_{uj,i}) \theta(q, \beta_{uj,i}), & p \leq \ell < M, \\ \frac{1}{N} \xi(\ell, p, k_{uj,i}, \beta_{uj,i}) \theta(q, \beta_{uj,i}) \phi(k, q, k_{uj,i}), & 0 \leq \ell < p, \end{cases} \end{aligned} \quad (9a)$$

$$\xi(\ell, p, k_{uj,i}, \beta_{uj,i}) = e^{j2\pi \left(\frac{\ell-p}{M} \right) \left(\frac{k_{uj,i} + \beta_{uj,i}}{N} \right)}, \quad (9b)$$

$$\theta(q, \beta_{uj,i}) = \frac{e^{-j2\pi(-q-\beta_{uj,i})} - 1}{e^{-j\frac{2\pi}{N}(-q-\beta_{uj,i})} - 1}, \quad (9c)$$

$$\phi(k, q, k_{uj,i}) = e^{-j2\pi \frac{[k-k_{uj,i}+q]_N}{N}}. \quad (9d)$$

The input-output relationship in (8) can be further column-wise vectorized as

$$\mathbf{y}_{uj} = \mathbf{H}_{uj} \tilde{\mathbf{x}}_j, \quad (10)$$

where $\tilde{\mathbf{x}}_j, \mathbf{y}_{uj} \in \mathbb{C}^{MN \times 1}$, and $\mathbf{H}_{uj} \in \mathbb{C}^{MN \times MN}$ is a sparse matrix.

Consequently, the observations obtained at u -th RRH can be expressed as

$$\bar{\mathbf{y}}_u = \sum_{j=1}^J \sqrt{P_j} \mathbf{H}_{uj} \tilde{\mathbf{x}}_j + \boldsymbol{\omega}_u, \quad u = 1, 2, \quad (11)$$

where $\boldsymbol{\omega}_u \in \mathbb{C}^{MN \times 1} \sim \mathcal{CN}(\mathbf{0}, N_0 \mathbf{I})$ is the complex additive white Gaussian noise (AWGN) at u -th RRH, and P_j is the transmission power of j -th user. The basic block diagram of the considered system is illustrated in Fig. 3.

III. PERFORMANCE ANALYSIS

As shown by [24], [42], [43] and the results of this section, the single-user ABER performance bound can actually be regarded as the benchmark of the ABER performance for the multi-user scenario with the optimal ML detector. In order to make the analysis tractable, in this section, we analyze the single-user PEP and characterize its ABER bound as the benchmark of our OBSCMA with CoMP system.

When the proposed OBSCMA with CoMP system supports only a single user (j -th user is considered here without loss of generality), the received signal at u -th RRH in (11) can be rewritten in an alternate form as

$$\bar{\mathbf{y}}_u = \sqrt{P_j \times PL(d_{uj})} \boldsymbol{\Phi}^{(u)}(\mathbf{X}_j) \mathbf{h}_{uj} + \boldsymbol{\omega}_u, \quad u = 1, 2, \quad (12)$$

where $\mathbf{h}_{uj} = [h_{uj,1}, h_{uj,2}, \dots, h_{uj,L_{uj}}]^T \in \mathbb{C}^{L_{uj} \times 1}$ is the channel coefficient vector between the j -th user and u -th RRH, and $\boldsymbol{\Phi}^{(u)}(\mathbf{X}_j) \in \mathbb{C}^{MN \times L_{uj}}$ is referred to as the equivalent transmitted codeword matrix whose i -th row ($i = kM + \ell, i = 0, 1, \dots, MN - 1$) is given in (13), as shown at the top of the next page.

In order to investigate the theoretical error performance bound, we combine the equations in (12) as

$$\bar{\mathbf{y}} = \sqrt{P_j} \boldsymbol{\Phi}(\mathbf{X}_j) \mathbf{h}_j + \boldsymbol{\omega}, \quad (14)$$

where $\bar{\mathbf{y}} = [\bar{\mathbf{y}}_1^T, \bar{\mathbf{y}}_2^T]^T \in \mathbb{C}^{2MN \times 1}$, $\mathbf{h}_j = [\mathbf{h}_{1j}^T, \mathbf{h}_{2j}^T]^T \in \mathbb{C}^{(L_{1j}+L_{2j}) \times 1}$, $\boldsymbol{\omega} = [\boldsymbol{\omega}_1^T, \boldsymbol{\omega}_2^T]^T \in \mathbb{C}^{2MN \times 1}$, and

$$\boldsymbol{\Phi}(\mathbf{X}_j) = \begin{bmatrix} \sqrt{PL(d_{1j})} \boldsymbol{\Phi}^{(1)}(\mathbf{X}_j) & \mathbf{0} \\ \mathbf{0} & \sqrt{PL(d_{2j})} \boldsymbol{\Phi}^{(2)}(\mathbf{X}_j) \end{bmatrix} \in \mathbb{C}^{2MN \times (L_{1j}+L_{2j})}.$$

Assuming perfect CSI is available at the receiver, the conditional PEP, i.e., the probability of transmitting \mathbf{X}_j but erroneously deciding on $\hat{\mathbf{X}}_j$, is given by

$$\begin{aligned} & \Pr(\mathbf{X}_j \rightarrow \hat{\mathbf{X}}_j | d_{1j}, d_{2j}, \mathbf{h}_j) \\ &= Q \left(\sqrt{\frac{\rho}{2}} \left\| \left(\boldsymbol{\Phi}(\mathbf{X}_j) - \boldsymbol{\Phi}(\hat{\mathbf{X}}_j) \right) \mathbf{h}_j \right\|^2 \right), \end{aligned} \quad (15)$$

where $Q(x)$ is the tail distribution function of the standard Gaussian distribution and $\rho = P_j/N_0$.

By resorting the approximation $Q(x) \approx \frac{1}{12} \exp(-x^2/2) + \frac{1}{4} \exp(-2x^2/3)$, we can rewrite (15) as

$$\begin{aligned} & \Pr(\mathbf{X}_j \rightarrow \hat{\mathbf{X}}_j | d_{1j}, d_{2j}, \mathbf{h}_j) \\ & \approx \frac{1}{12} \exp \left(-\frac{\rho \left\| \left(\boldsymbol{\Phi}(\mathbf{X}_j) - \boldsymbol{\Phi}(\hat{\mathbf{X}}_j) \right) \mathbf{h}_j \right\|^2}{4} \right) \\ & \quad + \frac{1}{4} \exp \left(-\frac{\rho \left\| \left(\boldsymbol{\Phi}(\mathbf{X}_j) - \boldsymbol{\Phi}(\hat{\mathbf{X}}_j) \right) \mathbf{h}_j \right\|^2}{3} \right). \end{aligned} \quad (16)$$

After averaging over the distances d_{1j} and d_{2j} , (16) can be approximately expressed as

$$\begin{aligned} & \Pr(\mathbf{X}_j \rightarrow \hat{\mathbf{X}}_j | \mathbf{h}_j) \\ & \approx \frac{1}{12} \exp \left(-\frac{\rho \left\| \left(\bar{\boldsymbol{\Phi}}(\mathbf{X}_j) - \bar{\boldsymbol{\Phi}}(\hat{\mathbf{X}}_j) \right) \mathbf{h}_j \right\|^2}{4} \right) \\ & \quad + \frac{1}{4} \exp \left(-\frac{\rho \left\| \left(\bar{\boldsymbol{\Phi}}(\mathbf{X}_j) - \bar{\boldsymbol{\Phi}}(\hat{\mathbf{X}}_j) \right) \mathbf{h}_j \right\|^2}{3} \right), \end{aligned} \quad (17)$$

where

$$\bar{\boldsymbol{\Phi}}(\mathbf{X}_j) = \begin{bmatrix} \sqrt{\mathbb{E}(PL(d_{1j}))} \boldsymbol{\Phi}^{(1)}(\mathbf{X}_j) & \mathbf{0} \\ \mathbf{0} & \sqrt{\mathbb{E}(PL(d_{2j}))} \boldsymbol{\Phi}^{(2)}(\mathbf{X}_j) \end{bmatrix},$$

and $\mathbb{E}(\cdot)$ represents expectation.

Note that $\left(\bar{\boldsymbol{\Phi}}(\mathbf{X}_j) - \bar{\boldsymbol{\Phi}}(\hat{\mathbf{X}}_j) \right)^H \left(\bar{\boldsymbol{\Phi}}(\mathbf{X}_j) - \bar{\boldsymbol{\Phi}}(\hat{\mathbf{X}}_j) \right)$ is a Hermitian matrix, its rank and the non-zero eigenvalues are defined as R and $\lambda_i, i = 1, 2, \dots, R$, respectively. Hence, we can obtain

$$\begin{aligned} & \left\| \left(\bar{\boldsymbol{\Phi}}(\mathbf{X}_j) - \bar{\boldsymbol{\Phi}}(\hat{\mathbf{X}}_j) \right) \mathbf{h}_j \right\|^2 \\ &= \mathbf{h}_j^H \left(\bar{\boldsymbol{\Phi}}(\mathbf{X}_j) - \bar{\boldsymbol{\Phi}}(\hat{\mathbf{X}}_j) \right)^H \left(\bar{\boldsymbol{\Phi}}(\mathbf{X}_j) - \bar{\boldsymbol{\Phi}}(\hat{\mathbf{X}}_j) \right) \mathbf{h}_j \\ &= \mathbf{h}_j^H \mathbf{U} \boldsymbol{\Sigma} \mathbf{U}^H \mathbf{h}_j \\ &= \tilde{\mathbf{h}}_j^H \tilde{\boldsymbol{\Sigma}} \tilde{\mathbf{h}}_j \\ &= \sum_{i=1}^R \lambda_i \left| \tilde{h}_{ji} \right|^2, \end{aligned} \quad (18)$$

where \mathbf{U} is a unitary matrix, $\tilde{\mathbf{h}}_j = \mathbf{h}_j^H \mathbf{U}$ and $\tilde{\boldsymbol{\Sigma}} = \text{diag}\{\lambda_1, \lambda_2, \dots, \lambda_{L_{1j}+L_{2j}}\}$.

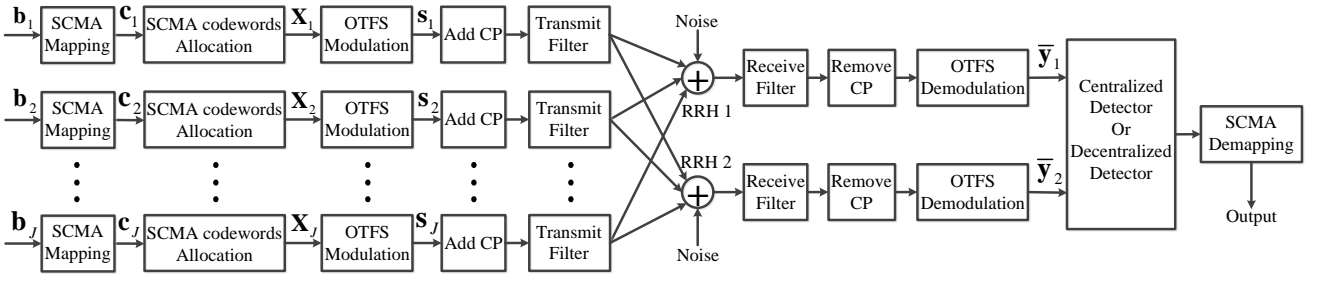


Fig. 3. Block diagram of the proposed OBSCMA with CoMP system.

$$\Phi_i^{(u)}(\mathbf{X}_j) = \begin{bmatrix} \sum_{p=0}^{P_{uj}-1} \sum_{q=0}^{N-1} P_{rc}(pT_s - t_{uj} - \tau_{uj,1})\gamma(k, \ell, p, q, k_{uj,1}, \beta_{uj,1})X_j [[\ell - p]_M, [k - k_{uj,1} + q]_N] \\ \sum_{p=0}^{P_{uj}-1} \sum_{q=0}^{N-1} P_{rc}(pT_s - t_{uj} - \tau_{uj,2})\gamma(k, \ell, p, q, k_{uj,2}, \beta_{uj,2})X_j [[\ell - p]_M, [k - k_{uj,2} + q]_N] \\ \vdots \\ \sum_{p=0}^{P_{uj}-1} \sum_{q=0}^{N-1} P_{rc}(pT_s - t_{uj} - \tau_{uj,L_{uj}})\gamma(k, \ell, p, q, k_{uj,L_{uj}}, \beta_{uj,L_{uj}})X_j [[\ell - p]_M, [k - k_{uj,L_{uj}} + q]_N] \end{bmatrix}^T. \quad (13)$$

Since $\tilde{\mathbf{h}}_j$ is obtained by multiplying a unitary matrix with \mathbf{h}_j^H , it has the same distribution as that of \mathbf{h}_j^H . The elements in $\tilde{\mathbf{h}}_j$ are assumed to be independent and identically distributed complex Gaussian random variables. Considering $\tilde{\mathbf{h}}_j \sim \mathcal{CN}(\mathbf{0}, \frac{2}{L_{1j}+L_{2j}}\mathbf{I}_{L_{1j}+L_{2j}})$, the final PEP is calculated by averaging (17) over the channel statistics and given by

$$\Pr(\mathbf{X}_j \rightarrow \hat{\mathbf{X}}_j) \approx \frac{1}{12} \prod_{i=1}^R \frac{1}{1 + \frac{\rho\lambda_i}{2(L_{1j}+L_{2j})}} + \frac{1}{4} \prod_{i=1}^R \frac{1}{1 + \frac{2\rho\lambda_i}{3(L_{1j}+L_{2j})}}. \quad (19)$$

As $\rho \rightarrow \infty$, (19) can be further simplified as

$$\Pr(\mathbf{X}_j \rightarrow \hat{\mathbf{X}}_j) \approx \left[\frac{1}{12} \left(\frac{\left(\prod_{i=1}^R \lambda_i \right)^{\frac{1}{R}}}{2(L_{1j}+L_{2j})} \right)^{-R} + \frac{1}{4} \left(\frac{2 \left(\prod_{i=1}^R \lambda_i \right)^{\frac{1}{R}}}{3(L_{1j}+L_{2j})} \right)^{-R} \right] \rho^{-R}. \quad (20)$$

From the above analysis, we conclude that the system diversity order is determined by R , which could be as high as the summation of the resolvable paths of the channels between the user and the RRHs. Consequently, according to the union bounding technique, the ABER of the single-user system can be upper bounded by

$$P_e \leq \frac{1}{JQ^{\frac{MN}{K}} \frac{MN}{K} \log_2 Q} \sum_{j=1}^J \sum_{\mathbf{X}_j} \sum_{\hat{\mathbf{X}}_j \neq \mathbf{X}_j} \Pr(\mathbf{X}_j \rightarrow \hat{\mathbf{X}}_j) e(\mathbf{X}_j, \hat{\mathbf{X}}_j), \quad (21)$$

where $e(\mathbf{X}_j, \hat{\mathbf{X}}_j)$ represents the number of bits in difference for the corresponding pairwise error event.

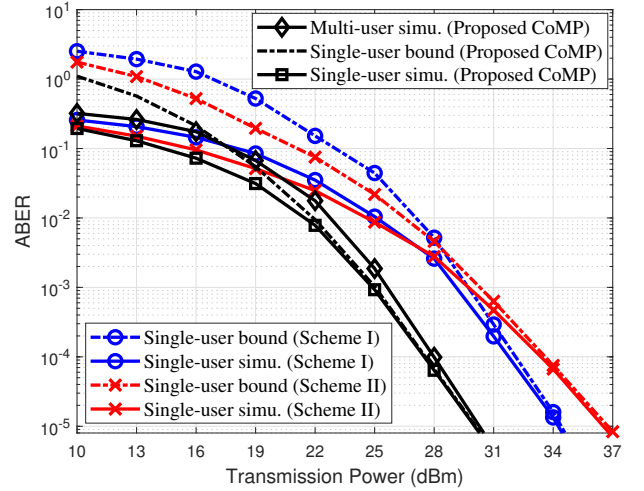


Fig. 4. ABER performance comparison for different scenarios.

In Fig. 4, we examine the effectiveness of the ABER performance analysis with ML detector. The user-specific codebooks are generated according to [44] with $J = 6$, $K = 4$, $D = 2$ and $Q = 4$. We consider a delay-Doppler plane with $M = 4$ and $N = 2$. The transmission power of each mobile user is assumed to be the same. Here, we select a typical urban channel model [45] with $L_{1j} = L_{2j} = L = 4$ resolvable paths for each user. The channel response for each mobile user is generated by using Jakes formulation [6], [41] with maximum Doppler frequency shift equals to 1111 Hz for the speed of 300 km/h. All the other simulation setups are the same as introduced in Section V. To highlight the superiority of the proposed scheme, we also provide the single-user benchmark performance of co-located RRHs scheme shown in Fig. 1(b) and traditional cellular network scheme shown in Fig. 1(c), denoted as Scheme I and Scheme II, respectively.

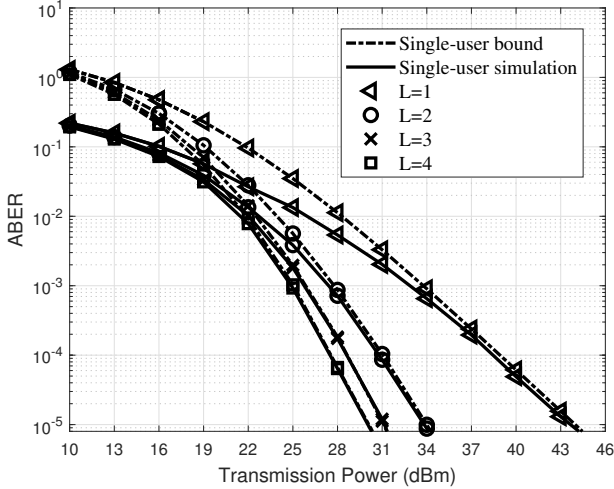


Fig. 5. ABER performance comparison with different resolvable paths.

From Fig. 4, we observe that the performance of single-user bound and single-user simulation tend to converge at high region of transmission power for each scheme. Compared to the single-user ABER bound of OBSCMA with CoMP system, the performance of the proposed multi-user simulation degrades in the low transmission power due to the CCI, and achieves a similar ABER result for the high transmission power. Hence, the ABER bound analysis are effective for single-user system and can be applied as the benchmark performance of our OBSCMA with CoMP system. We also notice that the ABER performance of Scheme I and Scheme II intersect with each other as the transmission power increases. The reason is because Scheme II achieves better performance in the low transmission power by leveraging the favorable propagation gain. However, the performance of Scheme I becomes better than Scheme II in the high transmission power due to its benefit of high spatial diversity gain.

Fig. 5 further illustrates the effect of the number of resolvable paths on the single-user ABER performance of OBSCMA with CoMP system. It is obvious that the ABER performance improves as L increases. This is due to the fact that high diversity gain can be obtained for better performance with large value of L . We again notice that the ABER performance of single-user bound is tight and approach that of single-user simulation for different L , which further exhibits the effectiveness of our ABER performance analysis.

IV. RECEIVER DESIGN

In the last section, we characterize the asymptotic single-user ABER performance as the benchmark of our proposed OBSCMA with CoMP system by PEP analysis based on ML detector. However, the complexity order of the ML is $\mathcal{O}\left(Q^{\frac{MNJ}{K}}\right)$, resulting in intolerable computational burden to the receiver for practical large dimensional systems with massive number of user connections. We now investigate practical receiver algorithms to recover the signal for each user from the receptions of the RRHs. To this end, we rewrite

the expression in (11) as

$$\bar{\mathbf{y}}_u = \bar{\mathbf{H}}_u \bar{\mathbf{x}} + \omega_u, \quad u = 1, 2, \quad (22)$$

where $\bar{\mathbf{H}}_u = [\sqrt{P_1} \mathbf{H}_{u1}, \sqrt{P_2} \mathbf{H}_{u2}, \dots, \sqrt{P_J} \mathbf{H}_{uJ}] \in \mathbb{C}^{MN \times MNJ}$, and $\bar{\mathbf{x}} = [\tilde{\mathbf{x}}_1^T, \tilde{\mathbf{x}}_2^T, \dots, \tilde{\mathbf{x}}_J^T]^T \in \mathbb{C}^{MNJ \times 1}$.

Note that $\bar{\mathbf{x}}$ is a sparse vector due to the sparse SCMA codewords. The number of non-zero entries in $\bar{\mathbf{x}}$ is only $\frac{MNJD}{K}$. Let $\hat{\mathbf{x}} \in \mathbb{C}^{\frac{MNJD}{K} \times 1}$ denotes the effective input after removing the zeros in $\bar{\mathbf{x}}$, and $\hat{\mathbf{H}}_u \in \mathbb{C}^{MN \times \frac{MNJD}{K}}$ represents the effective matrix after deleting the columns corresponding to the indices of zeros in $\bar{\mathbf{x}}$. Thus, we can simplify the relationship of (22) to

$$\bar{\mathbf{y}}_u = \hat{\mathbf{H}}_u \hat{\mathbf{x}} + \omega_u, \quad u = 1, 2. \quad (23)$$

As $\hat{\mathbf{x}}$ contains information from $\frac{MNJ}{K}$ SCMA codewords, we further group every D non-zero elements from the same SCMA codeword in $\hat{\mathbf{x}}$. Similarly, the corresponding columns in $\hat{\mathbf{H}}_u$ should be grouped together. We can now rewrite (23) as

$$\bar{\mathbf{y}}_u = \mathbf{H}_u \mathbf{x} + \omega_u, \quad u = 1, 2, \quad (24)$$

where $\mathbf{x} = [\mathbf{x}_1^T, \mathbf{x}_2^T, \dots, \mathbf{x}_{MNJ/K}^T]^T \in \mathbb{C}^{\frac{MNJD}{K} \times 1}$, $\mathbf{x}_c \in \mathbb{C}^{D \times 1}$, $\mathbf{h}_{d,c}^u \in \mathbb{C}^{1 \times D}$ and

$$\mathbf{H}_u = \begin{bmatrix} \mathbf{h}_{1,1}^u & \mathbf{h}_{1,2}^u & \cdots & \mathbf{h}_{1,MNJ/K}^u \\ \mathbf{h}_{2,1}^u & \mathbf{h}_{2,2}^u & \cdots & \mathbf{h}_{2,MNJ/K}^u \\ \vdots & \vdots & \ddots & \vdots \\ \mathbf{h}_{MN,1}^u & \mathbf{h}_{MN,2}^u & \cdots & \mathbf{h}_{MN,MNJ/K}^u \end{bmatrix} \in \mathbb{C}^{MN \times \frac{MNJD}{K}}.$$

From (24), we observe that the dimension of receptions at each RRH is less than the number of transmitted SCMA codewords as $J > K$. Hence, the conventional multi-user detection for orthogonal multiple access [14]–[16] cannot be directly applied in such an over-loaded system. To achieve better performance, the advanced receiver algorithms are required to recover the signal of each user. In the sequel, we develop the efficient centralized and decentralized detectors for multi-user detection, and also discuss their advantages and disadvantages, respectively.

A. Centralized Detector

In this subsection, we introduce the centralized detector to take advantage of the receptions from both RRHs. Specifically, the RRHs will forward their receptions to the BBU for centralized multi-user detection. We can combine the equations in (24) at the BBU as

$$\mathbf{y} = \mathbf{H} \mathbf{x} + \omega, \quad (25)$$

where $\mathbf{y} = [\bar{\mathbf{y}}_1^T, \bar{\mathbf{y}}_2^T]^T \in \mathbb{C}^{2MN \times 1}$, $\mathbf{H} = [\mathbf{H}_1^T, \mathbf{H}_2^T]^T \in \mathbb{C}^{2MN \times \frac{MNJD}{K}}$, and $\omega = [\omega_1^T, \omega_2^T]^T \in \mathbb{C}^{2MN \times 1}$.

Note that direct solution of (25) could be computationally complexity as it involves a large matrix inverse while MN can typically be in the order of thousands or even larger in OTFS system. Fortunately, we can use a sparsely connected factor graph to describe the linear model of (25) since \mathbf{H}

is a sparse matrix. The corresponding factor graph includes $2MN$ observation nodes y_d , $d = 1, 2, \dots, 2MN$, and $\frac{MNJ}{K}$ variable nodes \mathbf{x}_c , $c = 1, 2, \dots, \frac{MNJ}{K}$. An edge is connected between an observation node y_d and a variable node \mathbf{x}_c if $\mathbf{h}_{d,c} \neq \mathbf{0}_{1 \times D}$. Let $\mathcal{I}(d)$ and $\mathcal{J}(c)$ denote the index sets of non-zero components (i.e., $\mathbf{h}_{d,c} \neq \mathbf{0}_{1 \times D}$) in the d -th row and c -th column of \mathbf{H} , where $d = 1, 2, \dots, 2MN$ and $c = 1, 2, \dots, \frac{MNJ}{K}$, respectively. We also represent the corresponding numbers of non-zero components in the d -th row and c -th column as $|\mathcal{I}(d)|$ and $|\mathcal{J}(c)|$.

In general, one can derive an efficient MP algorithm [4], [6], [21] for symbol detection according to the sparse factor graph with low complexity. Here, we develop a customized GAEP detector for performance improvement. Recently, EP algorithm is widely applied to approximate the true posterior with modest complexity for traditional MIMO [46] and single carrier [47] systems. The performance advantage of EP motivates us to develop more efficient receiver algorithms in our model to overcome the co-channel user interference and the self-interference in the delay-Doppler domain. A detailed implementation of the centralized GAEP detector is summarized in **Algorithm 1**. We now describe its steps in iteration κ :

Algorithm 1 Centralized GAEP Detector

Input: $\bar{\mathbf{y}}_1, \bar{\mathbf{y}}_2, \mathbf{H}_1, \mathbf{H}_2, P_D(\mathbf{x})$ and n_c .

Initialization: $\boldsymbol{\mu}_{d,c}^{(0)}, \boldsymbol{\eta}_{d,c}^{(0)}$, $c = 1, 2, \dots, \frac{MNJ}{K}, d \in \mathcal{J}(c)$, $\delta_I^{(0)} = 0$ and iteration count $\kappa = 1$.

repeat

1) Each observation node y_d calculates the mean $C_{d,c}^{(\kappa)}[i]$ and variance $D_{d,c}^{(\kappa)}[i]$ in (27) and (28), and sends them to the connected variable nodes $\mathbf{x}_c, c \in \mathcal{I}(d)$ if $h_{d,c}[i] \neq 0, i = 1, 2, \dots, D$;

2) Each variable node \mathbf{x}_c generates the mean $\boldsymbol{\mu}_{d,c}^{(\kappa)}[i]$ and variance $\boldsymbol{\eta}_{d,c}^{(\kappa)}[i]$ in (32), and passes them back to the connected observation nodes $y_d, d \in \mathcal{J}(c)$ if $h_{d,c}[i] \neq 0, i = 1, 2, \dots, D$;

3) Compute the convergence indicator $\delta_I^{(\kappa)}$ in (33);

4) Update $P(\mathbf{x}) = \bar{P}^{(\kappa)}(\mathbf{x})$ if $\delta_I^{(\kappa)} > \delta_I^{(\kappa-1)}$;

5) $\kappa := \kappa + 1$;

until $\delta_I^{(\kappa)} = 1$ or $\kappa = n_c$.

Output: $P(\mathbf{x})$.

1) From observation node y_d to variable nodes $\mathbf{x}_c, c \in \mathcal{I}(d)$: At each observation node, we can express the received signal y_d as

$$y_d = \sum_{i=1, h_{d,c}[i] \neq 0}^D h_{d,c}[i] x_c[i] + \sum_{e \in \mathcal{I}(d), e \neq c} \mathbf{h}_{d,e} \mathbf{x}_e + \omega_d. \quad (26)$$

We approximate the messages updated and passed between the observation nodes and variable nodes on the factor graph as Gaussian. Hence, the observation node y_d sends the mean $C_{d,c}^{(\kappa)}[i]$ and variance $D_{d,c}^{(\kappa)}[i]$ to the variable node \mathbf{x}_c if

$h_{d,c}[i] \neq 0, i = 1, 2, \dots, D$, where

$$C_{d,c}^{(\kappa)}[i] = \frac{1}{h_{d,c}[i]} \left[y_d - \sum_{e \in \mathcal{I}(d), e \neq c} \mathbf{h}_{d,e} \boldsymbol{\mu}_{d,e}^{(\kappa-1)} - \sum_{\substack{f=1, f \neq i \\ h_{d,c}[f] \neq 0}}^D h_{d,c}[f] \boldsymbol{\mu}_{d,c}^{(\kappa-1)}[f] \right], \quad (27)$$

$$D_{d,c}^{(\kappa)}[i] = \frac{1}{|h_{d,c}[i]|^2} \left[\sum_{e \in \mathcal{I}(d), e \neq c} \sum_{f=1}^D |h_{d,e}[f]|^2 \boldsymbol{\eta}_{d,e}^{(\kappa-1)}[f] + \sum_{\substack{f=1, f \neq i \\ h_{d,c}[f] \neq 0}}^D |h_{d,c}[f]|^2 \boldsymbol{\eta}_{d,c}^{(\kappa-1)}[f] + \sigma^2 \right]. \quad (28)$$

Here, $\boldsymbol{\mu}_{d,e}^{(\kappa-1)}$ and $\boldsymbol{\eta}_{d,e}^{(\kappa-1)}$ are the mean and variance vectors received from variable node \mathbf{x}_e in the $(\kappa-1)$ -th iteration. They can be initialized in the first iteration by projecting the equiprobable symbols into Gaussian distribution as (30). σ^2 is the variance of the noise at the receiver input.

2) From variable node \mathbf{x}_c to observation nodes $y_d, d \in \mathcal{J}(c)$: The *a posteriori* probability can be expressed as follows at each variable node

$$\begin{aligned} & \bar{P}^{(\kappa)}(\mathbf{x}_c = \boldsymbol{\chi}_j) \\ & \propto P_D(\mathbf{x}_c = \boldsymbol{\chi}_j) \prod_{e \in \mathcal{J}(c)} \prod_{i=1, h_{e,c}[i] \neq 0}^D \exp \left(- \frac{|\chi_j[i] - C_{e,c}^{(\kappa)}[i]|^2}{D_{e,c}^{(\kappa)}[i]} \right), \\ & \forall \boldsymbol{\chi}_j \in \bar{\mathbb{A}}_j, \end{aligned} \quad (29)$$

where $j = \lceil \frac{cK}{MN} \rceil$ and $\lceil \cdot \rceil$ denotes the round up operation. $\bar{\mathbb{A}}_j$ is a set contains the non-zero elements of the predefined j -th user SCMA codebook \mathbb{A}_j , and $\boldsymbol{\chi}_j$ is a D -dimensional codeword from $\bar{\mathbb{A}}_j$. $P_D(\mathbf{x}_c = \boldsymbol{\chi}_j)$ represents the *a priori* probability when $\mathbf{x}_c = \boldsymbol{\chi}_j$, which can be assumed with equiprobable symbols if no priori information is observed. We then project this posteriori probability into a Gaussian distribution $\mathcal{CN}(E_c^{(\kappa)}[i], F_c^{(\kappa)}[i])$, $i = 1, 2, \dots, D$ and set a minimum allowed variance ε , i.e., $F_c^{(\kappa)}[i] = \max\{\varepsilon, F_c^{(\kappa)}[i]\}$ to avoid numerical instabilities. The mean $E_c^{(\kappa)}[i]$ and variance $F_c^{(\kappa)}[i]$ are given by

$$E_c^{(\kappa)}[i] = \sum_{\boldsymbol{\chi}_j \in \bar{\mathbb{A}}_j} \bar{P}^{(\kappa)}(\mathbf{x}_c = \boldsymbol{\chi}_j) \chi_j[i], \quad (30a)$$

$$F_c^{(\kappa)}[i] = \sum_{\boldsymbol{\chi}_j \in \bar{\mathbb{A}}_j} \bar{P}^{(\kappa)}(\mathbf{x}_c = \boldsymbol{\chi}_j) |\chi_j[i]|^2 - \left| E_c^{(\kappa)}[i] \right|^2. \quad (30b)$$

Following the Gaussian message combining rule [28], [47], we can update the extrinsic distribution $\bar{q}_E^{(\kappa)}(x_{d,c}[i]) \sim \mathcal{CN}(\bar{\boldsymbol{\mu}}_{d,c}^{(\kappa)}[i], \bar{\boldsymbol{\eta}}_{d,c}^{(\kappa)}[i])$ if $h_{d,c}[i] \neq 0, i = 1, 2, \dots, D$, where

$$\bar{\boldsymbol{\eta}}_{d,c}^{(\kappa)}[i] = \left[\left(F_c^{(\kappa)}[i] \right)^{-1} - \left(D_{d,c}^{(\kappa)}[i] \right)^{-1} \right]^{-1}, \quad (31a)$$

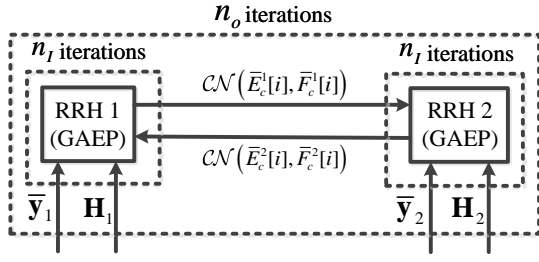


Fig. 6. Structure of the decentralized GAEP detector.

$$\bar{\mu}_{d,c}^{(\kappa)}[i] = \bar{\eta}_{d,c}^{(\kappa)}[i] \left[\frac{E_c^{(\kappa)}[i]}{F_c^{(\kappa)}[i]} - \frac{C_{d,c}^{(\kappa)}[i]}{D_{d,c}^{(\kappa)}[i]} \right]. \quad (31b)$$

Finally, the variable node \mathbf{x}_c calculates the mean $\mu_{d,c}^{(\kappa)}[i]$ and variance $\eta_{d,c}^{(\kappa)}[i]$ as follows and passes them back to the observation node y_d ,

$$\eta_{d,c}^{(\kappa)}[i] = \left[\frac{\Delta}{\bar{\eta}_{d,c}^{(\kappa)}[i]} + \frac{(1-\Delta)}{\eta_{d,c}^{(\kappa-1)}[i]} \right]^{-1}, \quad (32a)$$

$$\mu_{d,c}^{(\kappa)}[i] = \eta_{d,c}^{(\kappa)}[i] \left[\Delta \frac{\bar{\mu}_{d,c}^{(\kappa)}[i]}{\bar{\eta}_{d,c}^{(\kappa)}[i]} + (1-\Delta) \frac{\mu_{d,c}^{(\kappa-1)}[i]}{\eta_{d,c}^{(\kappa-1)}[i]} \right], \quad (32b)$$

where $\Delta \in (0, 1]$ is a message damping factor adopted to improve the performance and convergence. If the renewed variance $\eta_{d,c}^{(\kappa)}[i]$ is negative, we ignore the current update and utilize the value of previous iteration instead.

3) Convergence indicator: The convergence indicator $\delta_I^{(\kappa)}$ is defined as

$$\delta_I^{(\kappa)} = \frac{K}{MNJ} \sum_{c=1}^{MNJ/K} \mathbb{I} \left(\max_{\mathbf{x}_j \in \bar{\mathbb{A}}_j} \bar{P}^{(\kappa)}(\mathbf{x}_c = \mathbf{x}_j) \geq 1 - \varrho \right), \quad (33)$$

$$j = \left\lfloor \frac{cK}{MN} \right\rfloor$$

for some small $\varrho > 0$ and $\mathbb{I}(\cdot)$ stands for the indicator function.

4) Update criterion: If $\delta_I^{(\kappa)} > \delta_I^{(\kappa-1)}$, we then update

$$P(\mathbf{x}_c) = \bar{P}^{(\kappa)}(\mathbf{x}_c), \quad c = 1, 2, \dots, \frac{MNJ}{K}. \quad (34)$$

5) Terminating criterion: The centralized GAEP detector terminates if $\delta_I^{(\kappa)} = 1$ or the maximum iteration number n_c is reached.

We obtain the following decisions once the terminating criterion is satisfied

$$\hat{\mathbf{x}}_c = \arg \max_{\mathbf{x}_j \in \bar{\mathbb{A}}_j} P(\mathbf{x}_c = \mathbf{x}_j), \quad j = \left\lfloor \frac{cK}{MN} \right\rfloor, \quad c = 1, 2, \dots, \frac{MNJ}{K}. \quad (35)$$

Finally, the SCMA demapping is applied to recover the transmitted information bits of each user.

B. Decentralized Detector

As the two RRHs are also connected by the optical fibers directly, we can achieve a decentralized processing in a straightforward manner to enable the cooperation between these two RRHs. The structure of the decentralized detector is shown in Fig. 6. Specifically, the two RRHs apply the GAEP algorithm similar to **Algorithm 1** for symbol detection independently, and also exchange information iteratively to further improve the performance. After obtaining the extrinsic mean $\bar{E}_c^2[i]$ and variance $\bar{F}_c^2[i]$, $i = 1, 2, \dots, D, c = 1, 2, \dots, \frac{MNJ}{K}$ from the second RRH, the *a priori* probability is updated at the first RRH as

$$P_D(\mathbf{x}_c = \mathbf{x}_j) \propto \prod_{i=1}^D \exp \left(-\frac{|\chi_j[i] - \bar{E}_c^2[i]|^2}{\bar{F}_c^2[i]} \right), \quad \forall \mathbf{x}_j \in \bar{\mathbb{A}}_j, \quad (36)$$

$$j = \left\lfloor \frac{cK}{MN} \right\rfloor, \quad c = 1, 2, \dots, \frac{MNJ}{K}.$$

By applying GAEP algorithm for a certain number n_I of iterations, the first RRH projects the output probabilities $P(\mathbf{x}_c^1)$ into the *a posteriori* Gaussian distribution $\mathcal{CN}(E_c^1[i], F_c^1[i])$, $i = 1, 2, \dots, D, c = 1, 2, \dots, \frac{MNJ}{K}$ as (30).

The extrinsic mean $\bar{E}_c^1[i]$ and variance $\bar{F}_c^1[i]$ can be calculated as follows and then delivered to the second RRH,

$$\bar{F}_c^1[i] = \left[(F_c^1[i])^{-1} - (\bar{F}_c^2[i])^{-1} \right]^{-1}, \quad (37a)$$

$$\bar{E}_c^1[i] = \bar{F}_c^1[i] \left[\frac{E_c^1[i]}{F_c^1[i]} - \frac{\bar{E}_c^2[i]}{\bar{F}_c^2[i]} \right]. \quad (37b)$$

Similarly, the second RRH first updates the *a priori* probability $P_D(\mathbf{x}_c)$, and then produces the *a posteriori* Gaussian distribution for each symbol by using GAEP algorithm with n_I iterations. The extrinsic mean $\bar{E}_c^2[i]$ and variance $\bar{F}_c^2[i]$, $i = 1, 2, \dots, D, c = 1, 2, \dots, \frac{MNJ}{K}$ are finally generated and passed back to the first RRH to form the iterative loop. After a certain number n_o of iterations, each RRH obtains a final decision of $\hat{\mathbf{x}}$ in the last iteration step. A detailed implementation of the decentralized GAEP detector is summarized in **Algorithm 2**.

C. Discussion

We can observe that both centralized and decentralized detectors are efficient to recover the signal of each user. The centralized detector requires the RRHs to forward their receptions to the BBU and the decentralized detector requires frequent communications between the RRHs. We now discuss in details about their advantages and disadvantages, respectively.

From the algorithm discussion, the complexity of the proposed centralized and decentralized detectors are mainly determined by the GAEP algorithm. For each main loop iteration of the GAEP algorithm, (27)-(32) have a complexity order $\mathcal{O}(\bar{S}D)$, $\mathcal{O}(\bar{S}D)$, $\mathcal{O}(\bar{S}DQ)$, $\mathcal{O}\left(\frac{2MNJDQ}{K}\right)$, $\mathcal{O}(2\bar{S}D)$ and $\mathcal{O}(2\bar{S}D)$, respectively. Here, we write $\sum_{d=1}^{2MN} |\mathcal{I}(d)| =$

$\sum_{c=1}^{MNJ/K} |\mathcal{J}(c)| = \bar{S}$ for conciseness. Therefore, the overall

Algorithm 2 Decentralized GAEP Detector

Input: $\bar{\mathbf{y}}_1, \bar{\mathbf{y}}_2, \mathbf{H}_1, \mathbf{H}_2, n_I$ and n_o .
 Initialization: $\bar{\mathbf{E}}^u$ and $\bar{\mathbf{F}}^u, u = \{1, 2\}$.
for $\mathcal{T} = 0, 1, \dots, n_o$ **do**
 for $u = 1, 2$ **do** {parallel computing}
 1) Update $P_D(\mathbf{x})$ as in (36);
 2) Obtain the output probabilities $P(\mathbf{x}^u)$ by employing GAEP algorithm with n_I iterations;
 3) Project $P(\mathbf{x}^u)$ into Gaussian distribution $\mathcal{CN}(E_c^u[i], F_c^u[i]), i = 1, 2, \dots, D, c = 1, 2, \dots, \frac{MNJ}{K}$;
 4) Compute the extrinsic mean $\bar{E}_c^u[i]$ and variance $\bar{F}_c^u[i], i = 1, 2, \dots, D, c = 1, 2, \dots, \frac{MNJ}{K}$ as in (37);
 end for
 Exchange the extrinsic mean $\bar{\mathbf{E}}^u$ and variance $\bar{\mathbf{F}}^u$ between the two RRHs.
end for
 Output: $P(\mathbf{x}^u), u = \{1, 2\}$.

complexity orders are $n_c \mathcal{O}\left(6\bar{S}D + \bar{S}DQ + \frac{2MNJDQ}{K}\right)$ and $n_o n_I \mathcal{O}\left(6\bar{S}D + \bar{S}DQ + \frac{4MNJDQ}{K}\right)$ for centralized and decentralized detectors, respectively.³ From our simulations, we observe that the similar values of n_c and $n_o n_I$ are required to guarantee the algorithm convergence. Hence, our proposed centralized and decentralized detectors have comparable computational complexity.

However, the centralized detector may suffer from high communication overhead for information transfer between the RRHs and the BBU, especially when each RRH is with a large number of antennas. The amount of complex-valued data passed from each RRH to the BBU contains $MN N_u$ receptions and $3N_u L_u$ channel state information, where N_u represents the number of antennas at u -th RRH and $L_u = \sum_{j=1}^J L_{uj}, \forall u = \{1, 2\}$. The BBU then broadcasts $\frac{MNJD}{K}$ detected complex-valued data to each RRH afterwards. Therefore, the overall complex-valued data passed between the RRHs and the BBU in centralized detector is $MN(N_1 + N_2) + 3(N_1 L_1 + N_2 L_2) + \frac{2MNJD}{K}$. For the decentralized detector, the RRHs execute local computing processing parallelly, and coordinate with each other with limited consensus information exchange. The exchanged information only includes $\frac{MNJD}{K}$ means and $\frac{MNJD}{K}$ variances in each iteration, resulting in $\frac{2MNJD}{K} n_o$ complex-valued data transferred among the RRHs overall. Such a small amount of data exchange can not only alleviate the excessively requirement on interconnection bandwidth among the decentralized RRHs, but also avoid the large data transfer between the RRHs and the BBU in the centralized detector.

In addition, the BBU is generally located far away from the RRHs, and requires a high computing capacity to solve the

³Note that our proposed centralized and decentralized GAEP detectors can also be applied for OFDM-SCMA counterpart. Similar computational complexity are required for the OFDM-SCMA scenario compared to those of OBSCMA scenario, where \bar{S} represents the approximate numbers of non-zero elements of the channel matrix in OFDM-SCMA scenario.

large dimension problem of multi-user detection. Therefore, the centralized detector results in high-latency communications and effects on user experience. Nevertheless, the computations can be carried out in a decentralized and parallel fashion between the two neighbouring RRHs in the decentralized detector, which leads to a relatively low-latency communication system.

Note that our decentralized detector is not a substitute for the centralized detector but a powerful complement. It enables processing at the edges (i.e., RRHs) while still offering the possibility to process at the cloud (i.e., BBU) if the backhaul bandwidth and computation are sufficient to support latency-tolerant applications. To summarize, we include the detailed comparisons of the centralized and decentralized detectors in TABLE I.

V. SIMULATION RESULTS

In this section, we evaluate the performance of our proposed centralized and decentralized detectors for OBSCMA with CoMP systems. In our simulations, the carrier frequency is centered at 4 GHz and subcarrier spacing $\Delta f = 15$ kHz. The rolloff factor of the RRC filters is set to 0.4 for both the transmitter and receiver. Unless otherwise specified, we consider a delay-Doppler plane with $M = 64$ and $N = 16$. We also assume that $J = 6$ users are sharing $K = 4$ orthogonal resources simultaneously, and set $D = 2$ non-zero entries in each codeword. The user-specific codebooks are designed according to [44] with size $Q = 4$, and the transmission power of each mobile user is assumed to be the same.

As shown in Fig. 1(a), we consider a scenario where the mobile users are uniformly and independently distributed in the cell. The RRHs are positioned along the highway, spacing each other by $d_h = 1000$ m. The perpendicular distance of the RRHs and the highway line $d_p = 150$ m, and the width distance of the highway road $d_w = 50$ m. The distance-dependent pathloss propagation is modeled as $PL(d)[\text{dB}] = 142.1 + 37.6 \log_{10}(d)$ [48], where d is the distance in kilometers. The noise power spectral density is set to be -174 dBm/Hz for both RRHs. We adopt a typical urban channel model [45] with exponential power delay profile. The velocity of the j -th mobile user is set to 300 km/h, leading to a maximum Doppler frequency shift $\nu_{j,\max} = 1111$ Hz, $\forall j = \{1, 2, \dots, J\}$. We further generate the Doppler frequency shift for the i -th delay of the channel between the j -th user and u -th RRH by using the Jakes formulation [6], [41], i.e., $\nu_{uj,i} = \nu_{j,\max} \cos(\rho_{uj,i})$, where $\rho_{uj,i}$ is uniformly distributed over $[\frac{\pi}{2}, \pi]$ if the j -th user is moving away from the u -th RRH, and distributed over $[0, \frac{\pi}{2}]$ if the j -th user is moving towards the u -th RRH.

We assume that the full CSIs are known at the receiver and also test the effect of channel uncertainties on receiver performance. After extensive experimentations, we select $\Delta = 0.3$, $\varepsilon = 10^{-8}$, $\varrho = 0.1$ and $n_c = 20$ to yield attractive compromise between convergence speed and accuracy. The simulation results are average over 1000 independent Monte Carlo trials.

We first investigate the effects of SCMA codewords allocation on receiver performance. Fig. 7 illustrates the ABER

TABLE I. Detailed comparisons of the centralized and decentralized detectors.

Detectors	Computational Complexity	Communication Overhead	Latency
Centralized detector	$n_c \mathcal{O} \left(6\bar{S}D + \bar{S}DQ + \frac{2MNJDQ}{K} \right)$	$MN(N_1 + N_2) + 3(N_1L_1 + N_2L_2) + \frac{2MNJD}{K}$	High
Decentralized detector	$n_o n_I \mathcal{O} \left(6\bar{S}D + \bar{S}DQ + \frac{4MNJDQ}{K} \right)$	$\frac{2MNJD}{K} n_o$	Low

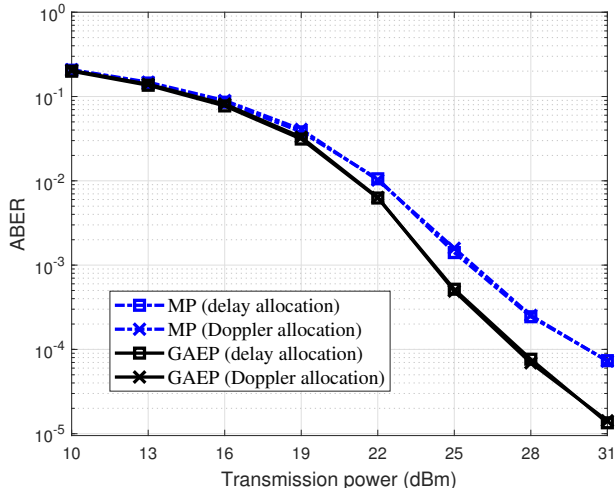


Fig. 7. ABER performance comparison for different SCMA codewords allocations and detection algorithms.

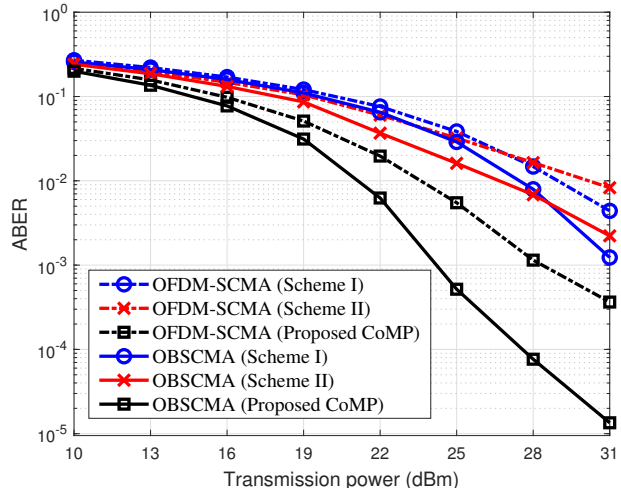


Fig. 8. ABER performance comparison for different scheme scenarios.

performance of the proposed OBSCMA with CoMP system for different SCMA codewords allocations. Without loss of generality, we apply centralized GAEP detector and allocate the SCMA codewords either along the delay axis in Fig. 2(a) (denoted as delay allocation) or along the Doppler axis in Fig. 2(b) (denoted as Doppler allocation). To highlight the superiority of the proposed GAEP algorithm, we also provide the baseline performance of traditional MP algorithm [4], [6] in Fig. 7. We can observe that the proposed GAEP algorithm outperforms the MP algorithm in the considered OBSCMA with CoMP system. We also notice that the SCMA codewords allocation has slightly effect on the receiver performance. In the rest of our simulations, we shall allocate the SCMA codewords along the delay axis unless otherwise noted.

Fig. 8 compares the ABER performance of the proposed scheme with those of co-located RRHs scheme shown in Fig. 1(b) and traditional cellular network scheme shown in Fig. 1(c), denoted as Scheme I and Scheme II, respectively. We also produce the performance of traditional OFDM-SCMA counterparts as benchmarks for different schemes in Fig. 8. Note that the proposed GAEP algorithm can be generalized to the OFDM-SCMA scenarios in a straightforward manner, thus, we omit the details here for brevity. The results reveal that all the receivers benefit from higher transmission power. The OBSCMA can achieve better performance than its OFDM-SCMA counterparts for each scheme. Our proposed OBSCMA with CoMP system outperforms the other schemes significantly owing to the utilization of sufficient underlying channel diversity.

We also note that as transmission power increases, the ABER performance of Scheme I and Scheme II intersect

with each other for both the OBSCMA and OFDM-SCMA scenarios. This is due to the fact that Scheme II experiences favorable propagation gain but limits to the spatial diversity gain.

Fig. 9 shows the ABER performance of our proposed centralized and decentralized detectors for OBSCMA with CoMP system. The results clearly show that the ABER performance of decentralized detector with sufficient number of iterations would asymptotically approach that of centralized detector. To guarantee the convergence of decentralized detector, a larger iteration number n_I requires a relatively smaller value of n_o , and vice versa, i.e., a smaller number n_I demands a larger value of n_o . Therefore, our proposed decentralized detector can yield desirable trade-off between the local processing efficiency of each RRH and the communication overhead between the RRHs.

In Fig. 10, we test the ABER performance of the proposed centralized and decentralized detectors for OBSCMA with CoMP system under different user mobile velocities. We also present the performance of centralized detector for OFDM-SCMA counterpart as benchmark. As the velocities of the mobile users grow, the ABER performance of our centralized and decentralized detectors for OBSCMA with CoMP system improves gradually and saturates after velocity beyond 600 km/h, particularly for high transmission power. This is attributed to the reason that OTFS modulation can resolve more distinct paths in the Doppler domain with the help of higher user velocity. As a result, better performance becomes possible. However, the performance improvement of OFDM-SCMA counterpart is negligible as the OFDM modulation cannot efficiently exploit the Doppler diversity. We again notice that the ABER performance of decentralized

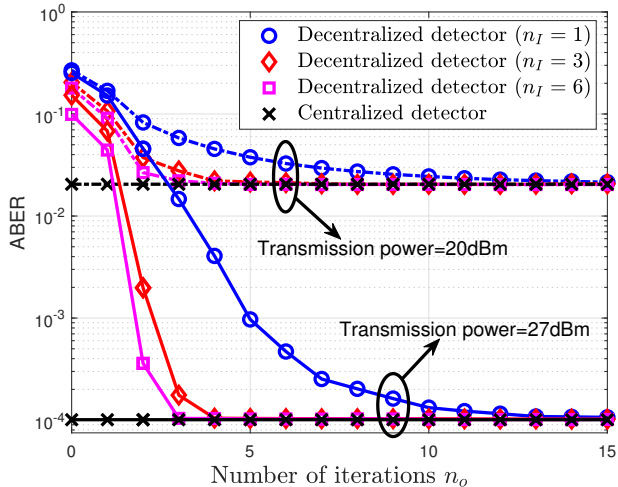


Fig. 9. ABER performance comparison of the proposed centralized and decentralized detectors.

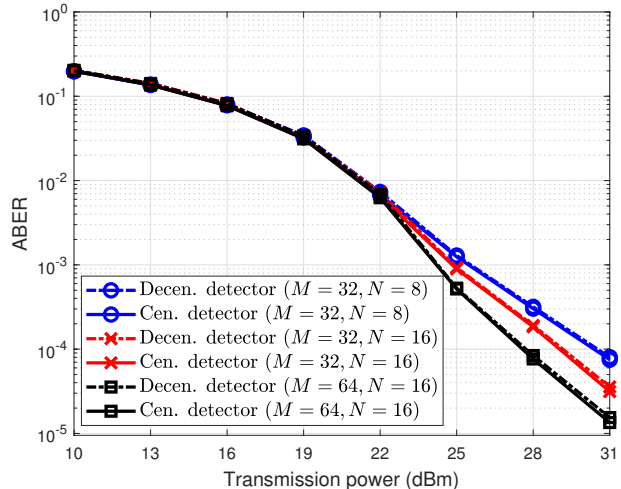


Fig. 11. ABER performance comparison for different system settings of M and N ($n_I = 3$ and $n_o = 5$).

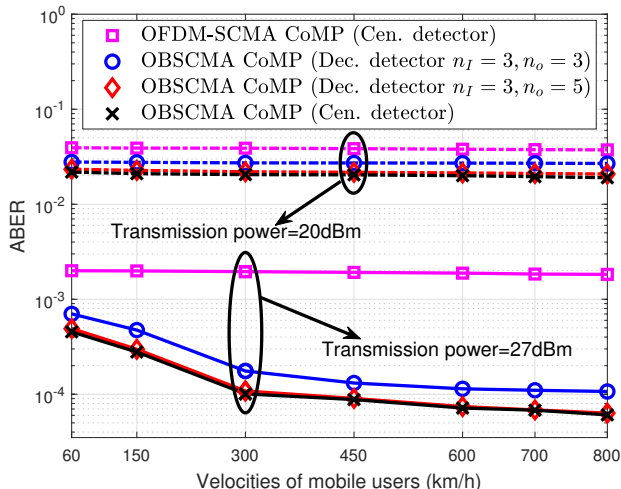


Fig. 10. ABER performance of centralized and decentralized detectors with different user mobile velocities.

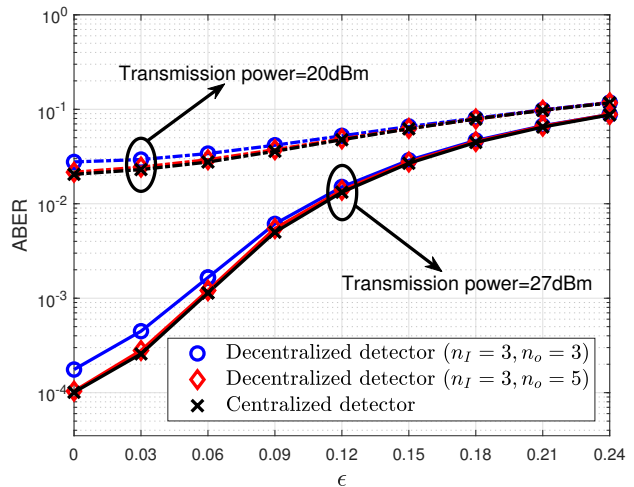


Fig. 12. ABER performance of centralized and decentralized detectors with imperfect CSIs.

detector approach that of centralized one for our OBSCMA with CoMP system when the iteration numbers are sufficient, and slightly degrade when the iteration numbers are inadequate for different velocities.

Fig. 11 further illustrates the ABER performance for both the centralized and decentralized detectors (with $n_I = 3$ and $n_o = 5$) under different system settings of M and N . We notice that the ABER performance of both centralized and decentralized detectors improve as M and N increase due to the higher resolution of OTFS delay-Doppler grid. This leads to the diversity benefit as the receiver can resolve a larger number of signal paths in the channel.

Finally, we test the effect of imperfect CSIs on the ABER performance of the proposed centralized and decentralized detectors in Fig. 12. Here, we capture the imperfect information of CSIs by adopting the following norm-bounded uncertainty

model [41]:

$$\begin{aligned} h_{uj,i} &= \hat{h}_{uj,i} + \Delta h_{uj,i}, \quad \|\Delta h_{uj,i}\| \leq \epsilon_{h_{uj,i}}, \\ \tau_{uj,i} &= \hat{\tau}_{uj,i} + \Delta \tau_{uj,i}, \quad \|\Delta \tau_{uj,i}\| \leq \epsilon_{\tau_{uj,i}}, \\ \nu_{uj,i} &= \hat{\nu}_{uj,i} + \Delta \nu_{uj,i}, \quad \|\Delta \nu_{uj,i}\| \leq \epsilon_{\nu_{uj,i}}, \end{aligned}$$

where $\hat{h}_{uj,i}$, $\hat{\tau}_{uj,i}$ and $\hat{\nu}_{uj,i}$ are the estimated values of $h_{uj,i}$, $\tau_{uj,i}$ and $\nu_{uj,i}$, respectively. $\Delta h_{uj,i}$, $\Delta \tau_{uj,i}$ and $\Delta \nu_{uj,i}$ represent the corresponding channel estimation errors, which are norm-bounded by the given radius $\epsilon_{h_{uj,i}}$, $\epsilon_{\tau_{uj,i}}$ and $\epsilon_{\nu_{uj,i}}$, respectively. For simplicity, we assume that $\epsilon_{h_{uj,i}} = \epsilon \|\hat{h}_{uj,i}\|$, $\epsilon_{\tau_{uj,i}} = \epsilon \|\hat{\tau}_{uj,i}\|$ and $\epsilon_{\nu_{uj,i}} = \epsilon \|\hat{\nu}_{uj,i}\|$, $\forall u, j, i$. From the results in Fig. 12, we observe that the performance degradation of our proposed centralized and decentralized detectors is mild for modest levels of channel uncertainty ϵ . As the receiver performance gradually drops in accordance with the levels of channel uncertainty, our proposed schemes and detectors exhibit robustness against typical CSI errors.

VI. CONCLUSION

In this paper, we proposed an OBSCMA with CoMP system, where a group of SCMA mobile users modulated in accordance with OTFS, and served by the RRH in front of them and the RRH behind them at the same time. The proposed OBSCMA with CoMP framework can efficiently support massive mobile connectivity and naturally harvest sufficient diversity for better performance. Based on the ML detector, we analyzed the single-user ABER bound as the benchmark of our OBSCMA with CoMP system. We also developed practical receiver algorithms for centralized and decentralized detectors to exploit the underlying channel diversity from the receptions of the RRHs. Our results demonstrated the superiority of the proposed OBSCMA with CoMP system compared to existing solutions, such as co-located RRHs and traditional cellular networks, as well as their OFDM-SCMA counterparts. The proposed centralized and decentralized detectors are both effectiveness and robustness against CSI uncertainty. The interesting future works include the coordinated design for more densely deployment of RRHs, the development of fast handover and efficient resource management, efficient robust receiver design based on realistic channels, grant-free random access for massive machine-type vehicle connectivity and so on.

REFERENCES

- [1] S. Yoo, D. González G., J. Hämäläinen, and K. Kim, "Doppler spectrum analysis of a roadside scatterer model for vehicle-to-vehicle channels: An indirect method," *IEEE Trans. Wireless Commun.*, vol. 17, no. 12, pp. 8007–8021, Dec. 2018.
- [2] R. Hadani, S. Rakib, M. Tsatsanis, A. Monk, A. J. Goldsmith, A. F. Molisch, and R. Calderbank, "Orthogonal time frequency space modulation," in *Proc. IEEE Wireless Commun. Netw. Conf. (WCNC)*, San Francisco, CA, USA, Mar. 2017, pp. 1–6.
- [3] W. Shen, L. Dai, J. An, P. Fan, and R. W. Heath, "Channel estimation for orthogonal time frequency space (OTFS) massive MIMO," *IEEE Trans. Signal Process.*, vol. 67, no. 16, pp. 4204–4217, Aug. 2019.
- [4] H. B. Mishra, P. Singh, A. K. Prasad, and R. Budhiraja, "OTFS channel estimation and data detection designs with superimposed pilots," *IEEE Trans. Wireless Commun.*, 2021.
- [5] M. Li, S. Zhang, Y. Ge, F. Gao, and P. Fan, "Joint channel estimation and data detection for hybrid RIS aided millimeter wave OTFS systems," *IEEE Trans. Commun.*, vol. 70, no. 10, pp. 6832–6848, Oct. 2022.
- [6] P. Raviteja, K. T. Phan, Y. Hong, and E. Viterbo, "Interference cancellation and iterative detection for orthogonal time frequency space modulation," *IEEE Trans. Wireless Commun.*, vol. 17, no. 10, pp. 6501–6515, Oct. 2018.
- [7] Z. Yuan, F. Liu, W. Yuan, Q. Guo, Z. Wang, and J. Yuan, "Iterative detection for orthogonal time frequency space modulation with unitary approximate message passing," *IEEE Trans. Wireless Commun.*, vol. 21, no. 2, pp. 714–725, Feb. 2022.
- [8] L. Xiang, Y. Liu, L.-L. Yang, and L. Hanzo, "Gaussian approximate message passing detection of orthogonal time frequency space modulation," *IEEE Trans. Veh. Tech.*, vol. 70, no. 10, pp. 10999–11004, Oct. 2021.
- [9] T. Thaj and E. Viterbo, "Low complexity iterative rake decision feedback equalizer for zero-padded OTFS systems," *IEEE Trans. Veh. Tech.*, vol. 69, no. 12, pp. 15606–15622, Dec. 2020.
- [10] G. Surabhi, R. M. Augustine, and A. Chockalingam, "On the diversity of uncoded OTFS modulation in doubly-dispersive channels," *IEEE Trans. Wireless Commun.*, vol. 18, no. 6, pp. 3049–3063, Jun. 2019.
- [11] P. Raviteja, Y. Hong, E. Viterbo, and E. Biglieri, "Effective diversity of OTFS modulation," *IEEE Wireless Commun. Lett.*, vol. 9, no. 2, pp. 249–253, Feb. 2020.
- [12] P. Singh, K. Yadav, H. B. Mishra, and R. Budhiraja, "BER analysis for OTFS zero forcing receiver," *IEEE Trans. Commun.*, 2022.
- [13] S. Li, J. Yuan, W. Yuan, Z. Wei, B. Bai, and D. W. K. Ng, "Performance analysis of coded OTFS systems over high-mobility channels," *IEEE Trans. Wireless Commun.*, vol. 20, no. 9, pp. 6033–6048, Sep. 2021.
- [14] V. Khammammetti and S. K. Mohammed, "OTFS-based multiple-access in high Doppler and delay spread wireless channels," *IEEE Wireless Commun. Lett.*, vol. 8, no. 2, pp. 528–531, Apr. 2019.
- [15] R. M. Augustine and A. Chockalingam, "Interleaved time-frequency multiple access using OTFS modulation," in *Proc. IEEE 90th Veh. Tech. Conf. (VTC2019-Fall)*, Honolulu, HI, USA, Sep. 2019, pp. 1–5.
- [16] G. Surabhi, R. M. Augustine, and A. Chockalingam, "Multiple access in the delay-doppler domain using OTFS modulation," *arXiv preprint arXiv:1902.03415*, 2019.
- [17] Y. Sun, D. W. K. Ng, Z. Ding, and R. Schober, "Optimal joint power and subcarrier allocation for full-duplex multicarrier non-orthogonal multiple access systems," *IEEE Trans. Commun.*, vol. 65, no. 3, pp. 1077–1091, Mar. 2017.
- [18] Z. Ding, F. Adachi, and H. V. Poor, "The application of MIMO to non-orthogonal multiple access," *IEEE Trans. Wireless Commun.*, vol. 15, no. 1, pp. 537–552, Jan. 2016.
- [19] Z. Ding, X. Lei, G. K. Karagiannidis, R. Schober, J. Yuan, and V. K. Bhargava, "A survey on non-orthogonal multiple access for 5G networks: Research challenges and future trends," *IEEE J. Sel. Areas Commun.*, vol. 35, no. 10, pp. 2181–2195, Oct. 2017.
- [20] L. Dai, B. Wang, Y. Yuan, S. Han, I. Chih-Lin, and Z. Wang, "Non-orthogonal multiple access for 5G: Solutions, challenges, opportunities, and future research trends," *IEEE Commun. Mag.*, vol. 53, no. 9, pp. 74–81, Sep. 2015.
- [21] J. Dai, K. Niu, and J. Lin, "Iterative Gaussian-approximated message passing receiver for MIMO-SCMA system," *IEEE Journal of Selected Topics in Signal Processing*, vol. 13, no. 3, pp. 753–765, Jun. 2019.
- [22] W. Yuan, N. Wu, Q. Guo, Y. Li, C. Xing, and J. Kuang, "Iterative receivers for downlink MIMO-SCMA: Message passing and distributed cooperative detection," *IEEE Trans. Wireless Commun.*, vol. 17, no. 5, pp. 3444–3458, May 2018.
- [23] P. Wang, L. Liu, S. Zhou, G. Peng, S. Yin, and S. Wei, "Near-optimal MIMO-SCMA uplink detection with low-complexity expectation propagation," *IEEE Trans. Wireless Commun.*, vol. 19, no. 2, pp. 1025–1037, Feb. 2020.
- [24] Y. Liu, L.-L. Yang, P. Xiao, H. Haas, and L. Hanzo, "Spatial modulated multicarrier sparse code-division multiple access," *IEEE Trans. Wireless Commun.*, vol. 19, no. 1, pp. 610–623, Jan. 2020.
- [25] A. Chatterjee, V. Rangamgari, S. Tiwari, and S. S. Das, "Nonorthogonal multiple access with orthogonal time-frequency space signal transmission," *IEEE Syst. J.*, vol. 15, no. 1, pp. 383–394, Mar. 2021.
- [26] K. Deka, A. Thomas, and S. Sharma, "OTFS-SCMA: A code-domain NOMA approach for orthogonal time frequency space modulation," *IEEE Trans. Commun.*, vol. 69, no. 8, pp. 5043–5058, Aug. 2021.
- [27] Z. Ding, R. Schober, P. Fan, and H. V. Poor, "OTFS-NOMA: An efficient approach for exploiting heterogeneous user mobility profiles," *IEEE Trans. Commun.*, vol. 67, no. 11, pp. 7950–7965, Nov. 2019.
- [28] Y. Ge, Q. Deng, P. Ching, and Z. Ding, "OTFS signaling for uplink NOMA of heterogeneous mobility users," *IEEE Trans. Commun.*, vol. 69, no. 5, pp. 3147–3161, May 2021.
- [29] J. Mietzner, R. Schober, L. Lampe, W. H. Gerstacker, and P. A. Hoeher, "Multiple-antenna techniques for wireless communications—a comprehensive literature survey," *IEEE Commun. Surv. Tuts.*, vol. 11, no. 2, pp. 87–105, 2nd Quart., 2009.
- [30] J. Zhang, E. Björnson, M. Matthaiou, D. W. K. Ng, H. Yang, and D. J. Love, "Prospective multiple antenna technologies for beyond 5G," *IEEE J. Sel. Areas Commun.*, vol. 38, no. 8, pp. 1637–1660, Aug. 2020.
- [31] Y. Shan and F. Wang, "Low-complexity and low-overhead receiver for OTFS via large-scale antenna array," *IEEE Trans. Veh. Tech.*, vol. 70, no. 6, pp. 5703–5718, Jun. 2021.
- [32] S. Srivastava, R. K. Singh, A. K. Jagannatham, and L. Hanzo, "Bayesian learning aided simultaneous row and group sparse channel estimation in orthogonal time frequency space modulated MIMO systems," *IEEE Trans. Commun.*, vol. 70, no. 1, pp. 635–648, Jan. 2022.
- [33] H. Qu, G. Liu, M. A. Imran, S. Wen, and L. Zhang, "Efficient channel equalization and symbol detection for MIMO OTFS systems," *IEEE Trans. Wireless Commun.*, 2022.
- [34] D. Shi, W. Wang, L. You, X. Song, Y. Hong, X. Gao, and G. Fettweis, "Deterministic pilot design and channel estimation for downlink massive MIMO-OTFS systems in presence of the fractional doppler," *IEEE Trans. Wireless Commun.*, vol. 20, no. 11, pp. 7151–7165, Nov. 2021.
- [35] Y. Liu, S. Zhang, F. Gao, J. Ma, and X. Wang, "Uplink-aided high mobility downlink channel estimation over massive MIMO-OTFS system," *IEEE J. Sel. Areas Commun.*, vol. 38, no. 9, pp. 1994–2009, Sep. 2020.

- [36] P. Singh, A. Gupta, H. B. Mishra, and R. Budhiraja, "Low-complexity ZF/MMSE MIMO-OTFS receivers for high-speed vehicular communication," *IEEE Open J. Commun. Soc.*, vol. 3, pp. 209–227, 2022.
- [37] B. C. Pandey, S. K. Mohammed, P. Raviteja, Y. Hong, and E. Viterbo, "Low complexity precoding and detection in multi-user massive MIMO OTFS downlink," *IEEE Trans. Veh. Tech.*, vol. 70, no. 5, pp. 4389–4405, May 2021.
- [38] M. Li, S. Zhang, F. Gao, P. Fan, and O. A. Dobre, "A new path division multiple access for the massive MIMO-OTFS networks," *IEEE J. Sel. Areas Commun.*, vol. 39, no. 4, pp. 903–918, Apr. 2021.
- [39] D. Lee, H. Seo, B. Clerckx, E. Hardouin, D. Mazzaresse, S. Nagata, and K. Sayana, "Coordinated multipoint transmission and reception in LTE-advanced: deployment scenarios and operational challenges," *IEEE Commun. Mag.*, vol. 50, no. 2, pp. 148–155, Feb. 2012.
- [40] J. Lu, X. Chen, S. Liu, and P. Fan, "Location-aware ICI reduction in MIMO-OFDM downlinks for high-speed railway communication systems," *IEEE Trans. Veh. Tech.*, vol. 67, no. 4, pp. 2958–2972, Apr. 2018.
- [41] Y. Ge, Q. Deng, P. Ching, and Z. Ding, "Receiver design for OTFS with a fractionally spaced sampling approach," *IEEE Trans. Wireless Commun.*, vol. 20, no. 7, pp. 4072–4086, Jul. 2021.
- [42] S.-C. Lim, N. Kim, and H. Park, "Uplink SCMA system with multiple antennas," *IEEE Trans. Veh. Tech.*, vol. 66, no. 8, pp. 6982–6992, Aug. 2017.
- [43] J. Bao, Z. Ma, M. Xiao, Z. Ding, and Z. Zhu, "Performance analysis of uplink SCMA with receiver diversity and randomly deployed users," *IEEE Trans. Veh. Tech.*, vol. 67, no. 3, pp. 2792–2797, Mar. 2018.
- [44] K. Xiao, B. Xia, Z. Chen, B. Xiao, D. Chen, and S. Ma, "On capacity-based codebook design and advanced decoding for sparse code multiple access systems," *IEEE Trans. Wireless Commun.*, vol. 17, no. 6, pp. 3834–3849, Jun. 2018.
- [45] M. Failli, *Digital Land Mobile Radio Communications. COST 207*. European Communities, Luxembourg, 1989.
- [46] Z. Zhang, H. Li, Y. Dong, X. Wang, and X. Dai, "Decentralized signal detection via expectation propagation algorithm for uplink massive MIMO systems," *IEEE Trans. Veh. Tech.*, vol. 69, no. 10, pp. 11 233–11 240, Oct. 2020.
- [47] S. Şahin, A. M. Cipriano, C. Poulliat, and M.-L. Boucheret, "Iterative equalization with decision feedback based on expectation propagation," *IEEE Trans. Commun.*, vol. 66, no. 10, pp. 4473–4487, Oct. 2018.
- [48] M. Tao, E. Chen, H. Zhou, and W. Yu, "Content-centric sparse multicast beamforming for cache-enabled cloud RAN," *IEEE Trans. Wireless Commun.*, vol. 15, no. 9, pp. 6118–6131, Sep. 2016.



Yao Ge (Member, IEEE) received the Ph.D. degree in Electronic Engineering from The Chinese University of Hong Kong (CUHK), Shatin, Hong Kong, in 2021, and the M.Eng. degree (research) in Communication and Information System and the B.Eng. degree in Electronics and Information Engineering from Northwestern Polytechnical University (NPU), Xi'an, China, in 2016 and 2013, respectively. He is currently a Research Fellow with Continental-NTU Corporate Lab, Nanyang Technological University (NTU), Singapore. From October 2015 to

March 2016, he was a Visiting Scholar with the Department of Electrical and Computer Systems Engineering, Monash University, Melbourne, VIC, Australia. From April 2016 to August 2016, he was a Visiting Scholar with the Department of Computer, Electrical and Mathematical Science and Engineering, King Abdullah University of Science and Technology (KAUST), Thuwal, Saudi Arabia. From May 2019 to December 2019, he was a Visiting Scholar with the Department of Electrical and Computer Engineering, University of California at Davis (UC Davis), Davis, CA, USA. His current research interests include wireless communications and system design, Internet of Things, cognitive radio networks, automotive vehicle signal processing and communications, wireless network security, statistical signal processing, optimization and game theory. He received the Best Paper Award from the International Conference on Wireless Communications and Signal Processing (WCSP) 2022. He is the Founding Member of the IEEE ComSoc Special Interest Group (SIG) on OTFS and has served as the Co-Chair for the IEEE/CIC ICC 2022 Workshop on OTFS.



Qinwen Deng (Student Member, IEEE) received the B.Eng. degree in Electronic Information Engineering from the University of Science and Technology of China (USTC), Hefei, China, in 2018. He is currently pursuing the Ph.D. degree with the Department of Electrical and Computer Engineering, University of California at Davis (UC Davis), Davis, CA, USA. His current research interests include wireless communications and hypergraph signal processing.



David González G. (Senior Member, IEEE) received the master's degree in mobile communications and the Ph.D. degree in signal theory and communications from the Universitat Politècnica de Catalunya, Spain. He has served as a Postdoctoral Fellow with the Department of Communications and Networking, Aalto University, Finland, from 2014 to 2017. From 2017 to 2018, he served as a Research Engineer with the Panasonic Research and Development Center, Germany. Since 2018, he has been with Continental AG, Germany. He has

represented his previous and current company as delegate in the 3GPP for 5G standardization, mainly focused on physical layer aspects and vehicular communications. His research is focused on diverse aspects of cellular networks and wireless communications, including interference modeling and coordination, radio access modeling and optimization, resource allocation, and vehicular communications (V2X).



Yong Liang Guan (Senior Member, IEEE) obtained his Ph.D. degree from the Imperial College London, London, U.K., and Bachelor of Engineering with first class honours from the National University of Singapore, Singapore. He is currently a Professor of Communication Engineering with the School of Electrical and Electronic Engineering, Nanyang Technological University (NTU), Singapore, where he leads the Continental-NTU Corporate Lab and the successful deployment of the campus-wide NTU-NXP V2X Test Bed. His research interests broadly

include coding and signal processing for communication systems and data storage systems. He is an Editor of the IEEE TRANSACTIONS ON VEHICULAR TECHNOLOGY. He is also an Associate Vice President of NTU and a Distinguished Lecturer of the IEEE Vehicular Technology Society (2021–2023).



Zhi Ding (Fellow, IEEE) is with the Department of Electrical and Computer Engineering at the University of California at Davis (UC Davis), Davis, where he currently holds the position of distinguished professor. He received his Ph.D. degree in Electrical Engineering from Cornell University in 1990. From 1990 to 2000, he was a faculty member of Auburn University and later at The University of Iowa. Prof. Ding joined the College of Engineering at UC Davis in 2000. His major research interests and expertise cover the areas of wireless networking,

communications, signal processing, multimedia, and learning. Prof. Ding supervised over 30 PhD dissertations since joining UC Davis. His research team of enthusiastic researchers works very closely with industry to solve practical problems and contributes to technological advances. His team has collaborated with researchers around the world and welcomes self-motivated young talents as new members.

Prof. Ding is a Fellow of IEEE and currently serves as the Chief Information Officer and Chief Marketing Officer of the IEEE Communications Society. He was an associate editor for IEEE TRANSACTIONS ON SIGNAL PROCESSING from 1994-1997, 2001-2004, and an associate editor of IEEE SIGNAL PROCESSING LETTERS 2002-2005. He was a member of Technical Committee on Statistical Signal and Array Processing and a member of Technical Committee on Signal Processing for Communications (1994-2003). Prof. Ding was the General Chair of the 2016 IEEE International Conference on Acoustics, Speech, and Signal Processing and the Technical Program Chair of the 2006 IEEE Globecom. He was also an IEEE *Distinguished Lecturer* (Circuits and Systems Society, 2004-06, Communications Society, 2008-09). He served on as IEEE TRANSACTIONS ON WIRELESS COMMUNICATIONS Steering Committee Member (2007-2009) and its Chair (2009-2010). Prof. Ding is a coauthor of the textbook: *Modern Digital and Analog Communication Systems*, 5th edition, Oxford University Press, 2019. Prof. Ding received the IEEE Communication Society's WTC Award in 2012 and the IEEE Communication Society's Education Award in 2020.